Inter- and Intratumoral Disposition of Platinum in Solid Tumors after Administration of Cisplatin

William C. Zamboni,[1] Anne C. Gervais, Merrill J. Egorin, Jan H. M. Schellens, Deborah R. Hamburger, Brian J. Delauter, Amy Grim, Eleanor G. Zuhowski, Erin Joseph, Dick Pluim, Douglas M. Potter, and Julie L. Eiseman

Department of Pharmaceutical Sciences, School of Pharmacy, University of Pittsburgh, Pittsburgh, Pennsylvania 15213 [W. C. Z.]; Departments of Medicine [W. C. Z., M. J. E.] and Pharmacology [M. J. E., J. L. E.], School of Medicine, University of Pittsburgh, Pittsburgh, Pennsylvania 15213; Program of Molecular Therapeutics and Drug Discovery [W. C. Z., A. C. G., M. J. E., D. R. H., B. J. D., A. G., E. G. Z., E. J., J. L. E.] and Biostatistics Facility [D. M. P.], University of Pittsburgh Cancer Institute, Pittsburgh, Pennsylvania 15213; and Department of Experimental Therapy, The Netherlands Cancer Institute, Amsterdam, 1066 CX The Netherlands [J. H. M. S., D. P.]

ABSTRACT

One possible explanation for variable tumor response within a single patient may be related to delivery of chemotherapeutic agents to the tumors. Microdialysis was used to evaluate inter- and intratumoral disposition of unbound platinum (Pt) after cisplatin administration to mice bearing B16 murine melanoma tumors or H23 human NSCLC xenografts. Before i.v. dosing with cisplatin (3 or 10 mg/kg), microdialysis probes were placed into the right and left sides of each tumor, and serial extracellular fluid (ECF) samples were collected for 2 h. After microdialysis, tumor samples were obtained at each probe site to measure total Pt and Pt-DNA adducts. In a separate study, serial plasma samples ($n = 3$ mice/time point) were obtained between 5 min and 2 h. Unbound Pt in tumor ECF and plasma and total Pt in tumor homogenates were measured by flameless atomic absorption spectrophotometry. Pt-DNA adducts in tumor samples were measured via ^{32}P-postlabeling. Area under the plasma (AUC_P) and tumor ECF (AUC_{ECF}) concentration-time curves of unbound Pt were calculated. Factor VIII expression was measured by immunohistochemistry in tumor samples. After administration of 3 or 10 mg/kg of cisplatin to mice bearing B16 tumors, there was a proportional increase in AUC_{PL} with dose; however, there was not a proportional increase in AUC_{ECF}. There was a relatively high (30-fold) inter- and low (2.5-fold) intratumoral variability in AUC_{ECF}. AUC_{ECF} correlated better with Pt-DNA adduct formation than did total Pt concentration in tumors. There was no relationship between Factor VIII expression and Pt exposure in tumors. The variable penetration of Pt from plasma into tumor ECF may be associated with variable response of tumors.

INTRODUCTION

Major advances have been made in the use of cancer chemotherapy (1). However, most patients, especially patients diagnosed with solid tumors, fail to respond to initial treatment or relapse after an initial response (1). Thus, there is a need to identify factors associated with lack of response and to develop new treatment strategies that address those factors. The development of effective chemotherapeutic agents for the treatment of solid tumors depends, in part, on the ability of those agents to achieve cytotoxic drug concentrations or exposure within the tumor (2, 3).

It is currently unclear why within a patient with solid tumors, such as melanoma or NSCLC[2], there can be a reduction in the size of some tumors, whereas other tumors can progress during or after treatment, although the genetic composition of the tumors is similar (4). Such variable antitumor responses within a single patient may be associated with inherent differences in tumor vascularity, capillary permeability, and/or tumor interstitial pressure that result in variable delivery of anticancer agents to different tumor sites (2, 3). However, studies evaluating the intratumoral concentration of anticancer agents and factors affecting tumor exposure in preclinical models and patients are rare (3, 5, 6).

Microdialysis is an *in vivo* sampling technique used to study the pharmacokinetics and drug metabolism in the blood and ECF of various tissues (7–9). The use of microdialysis methodology to evaluate the disposition of anticancer agents in tumors is relatively new (3, 5, 6). Microdialysis has been used to evaluate the tumor disposition of 5-fluorouracil and carboplatin in patients with primary breast cancer lesions and melanoma, respectively (5, 6). These studies depict the clinical use of microdialysis in evaluating the tumor disposition of anticancer agents in patients with accessible tumors. Microdialysis is based on the diffusion of nonprotein-bound drugs from interstitial fluid across the semipermeable membrane of the microdialysis probe (7–9). Microdialysis provides a means to obtain serial

Received 2/8/02; revised 5/9/02; accepted 5/9/02.
The costs of publication of this article were defrayed in part by the payment of page charges. This article must therefore be hereby marked *advertisement* in accordance with 18 U.S.C. Section 1734 solely to indicate this fact.

[1] To whom requests for reprints should be addressed, at University of Pittsburgh Cancer Institute, Biomedical Science Tower, E-1040, 200 Lothrop Street, Pittsburgh, PA 15213. Phone: (412) 383-7093; Fax: (412) 624-7737; E-mail: zamboniwc@msx.upmc.edu.

[2] The abbreviations used are: NSCLC, non-small cell cancer; ECF, extracellular fluid; Pt, platinum; FAAS, flameless atomic absorption spectrophotometry; Pt-GG, platinum and two adjacent guanine; Pt-AG, platinum and adjacent adenines and guanine.

samples from tumor ECF samples from which a concentration-time profile can be determined within a single tumor (3, 5, 6, 8).

The objectives of this study were to evaluate the inter- and intratumoral disposition of Pt in B16 murine melanoma tumors and H23 human NSCLC xenografts after administration of cisplatin. To determine what factors affected Pt exposure in tumors, the relationship between tumor vascularity, as measured by Factor VIII expression, and Pt exposure in B16 tumors and H23 xenografts was evaluated. In addition, we evaluated the relationship between total Pt exposure in tumor extracts and unbound Pt in tumor ECF, and the formation of Pt-DNA adducts.

MATERIALS AND METHODS

Mice. All mice were handled in accordance with the Guide to the Care and Use of Laboratory Animals (10), and studies were approved by the Institutional Animal Care and Use Committee at the University of Pittsburgh Medical Center. Mice (female C57Bl/6 and C.B-17 SCID, 4–6 weeks of age, and specific pathogen-free) were obtained from the National Cancer Institute Animal Production Program (Frederick, MD) and were allowed to acclimate to the animal facilities at the University of Pittsburgh for 1 week before initiation of study. Mice were housed in microisolator cages and allowed Teklad LM-484 autoclavable rodent chow (Harlan Tekla Diets, Madison, WI) or ISDPRO RMH3000 irradiated rodent chow (PMI Nutrition International, Inc., Brentwood, MO) and water *ad libitum*. Body weights and tumor size were measured twice weekly and clinical observations were made twice daily.

Tumor Lines. B16 murine melanoma cells and H23 NSCLC tumor fragments were obtained from the Division of Cancer Treatment Tumor Repository (Frederick, MD) and were mouse antigen production test-negative. B16 and H23 tumors were passed in C57BL/6 and SCID mice, respectively, as ~25-mg fragments that were implanted s.c. in the right flank by aseptic techniques. Tumor volumes were calculated from the formula: length $\times$ width^2/2, where length is the largest diameter, and width is the smallest diameter perpendicular to the length (11). Pharmacokinetic and microdialysis studies were performed when the tumors were ~1000–1500 mm^3 (1–1.5 g) in size.

Formulation and Administration. Cisplatin was administered as a bolus via a tail vein over ~30 s. Mice bearing B16 murine melanoma tumors were given cisplatin at 3 or 10 mg/kg. Mice bearing H23 human NSCLC xenografts were given cisplatin at 10 mg/kg. Cisplatin was diluted to 0.3 and 1 mg/ml in 0.9% NaCl (USP; Baxter, Inc., Deerfield, IL) so that the 3 and 10 mg/kg doses could be delivered in 0.01 ml/g of body weight.

Sample Processing for Plasma and Tissue Pharmacokinetic Studies. Because of limited blood volume, plasma and tissue pharmacokinetic studies were performed in one group of mice, and microdialysis studies were performed in other groups of mice. For the pharmacokinetic studies, mice (n = 3/time point) were euthanized with carbon dioxide, and heparinized blood samples (~0.8–1 ml) were collected by cardiac puncture before treatment, and at 5 min and 0.25, 0.5, 0.75, 1, 1.5, and 2 h after cisplatin administration. Blood samples were centrifuged at 12,000 $\times$ g for 4 min. For the analysis of total Pt in plasma, the resulting plasma was decanted into screw top tubes, immediately frozen in liquid nitrogen, and stored at −70°C until analyzed. For analysis of unbound Pt in plasma, the plasma was immediately ultrafiltered by placing 50 μl of plasma into an Amicon Centrifree micropartition device (Amicon Division, W. R. Grace, Beverly, MA), which was then centrifuged at 2000 $\times$ g for 20 min at 4°C (12, 13). The resulting ultrafiltrates were stored at −70°C until analyzed. Unbound Pt in the ultrafiltrate and total Pt in the plasma were measured by FAAS (12, 13).

Tumor, liver, kidneys, and spleen were also obtained from each mouse used for the pharmacokinetic studies described above. Tissues were removed, weighed, frozen in liquid nitrogen, and stored at −70°C until analyzed. For analysis of total Pt, tissue samples were thawed, homogenized in PBS (tissue:PBS at 1:3 w/v), and the homogenate was analyzed for Pt using a FAAS (12, 13).

Determination of Unbound Pt in Tumor ECF and Total Pt and Pt-DNA Adducts in Tumors. To evaluate the variability in Pt exposure within a single tumor, dual microdialysis probe studies were performed in each tumor (3). Commercially available microdialysis probes (CMA 20, Stockholm, Sweden) with a molecular cutoff of M_r 20,000, membrane length of 4 mm, and outer diameter of 0.5 mm were used. Because of the molecular weight cutoff of the microdialysis probe, only Pt not bound to large plasma proteins, such as albumin, could cross the semipermeable membrane and be collected. Therefore, Pt samples collected by microdialysis from tumor ECF were defined as unbound Pt. The microdialysis probe was perfused using a microdialysis microperfusion pump (CMA 102, Stockholm, Sweden). Dialysate samples were collected using a microfraction collector (CMA 142, Stockholm, Sweden).

Before administration of cisplatin, microdialysis probes were placed at parallel sites on the left and right sides of each tumor (3, 5, 6). For implantation of the probes, mice were anesthetized with pentobarbital (75 mg/kg IP), a 2-mm incision was made in the skin at 3–4 mm from the right and left ends of the tumor, and probes were inserted 6 mm into the tumor (3). The incision sites were closed, and probes were held in place with surgical glue. Probe placement was confirmed at necropsy.

After probe placement, 45 min were allowed to elapse so that probe and tumor ECF could equilibrate (3, 8, 9). The *in vivo* recovery of Pt by each probe in each tumor was assessed according to the retrodialysis method (3, 8, 9). *In vivo* retrodialysis calibration was performed using a dialysis solution (Ringer's solution, USP with cisplatin at 0.5 μg/ml) perfused through the probe at 2 μl/min, and dialysate samples were collected by the microfraction collector every 12 min for 48 min. The perfusate flow rate and collection interval used were based on our previous *in vitro* calibration studies, preclinical studies, and assay sensitivity. After the retrodialysis procedure, a washout period was performed, during which Ringer's solution USP without cisplatin was perfused at 2 μl/min. During the washout, dialysate samples were collected every 12 min for 48 min. After administration of cisplatin, microdialysis sampling of tumor ECF was performed every 12 min for 120 min. The concentration measured in each 12-min sample represented the average concentration of that interval, and thus the time of the sample was defined as the midpoint of that interval (*i.e.*, 0.1, 0.3, 0.5,

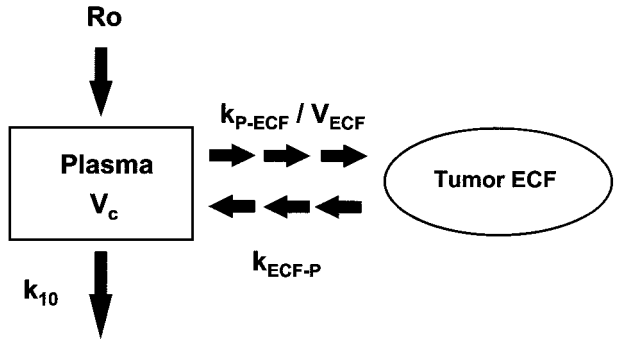

Fig. 1 Pharmacokinetic model with uncoupled distribution of the plasma and tumor compartments. The plasma concentration *versus* time profile and tumor ECF concentration *versus* time profiles were modeled separately. The parameters describing the unbound Pt plasma concentration *versus* time profile were volume of the central compartment (V_c) and elimination rate constant (k_{10}). The parameters describing the unbound Pt tumor ECF concentration-time profile were the rate constant describing the movement of drug from the plasma to tumor ECF ($k_{P\text{-}ECF}/V_{ECF}$) and rate constant describing the movement of drug from the tumor ECF ($k_{ECF\text{-}P}$).

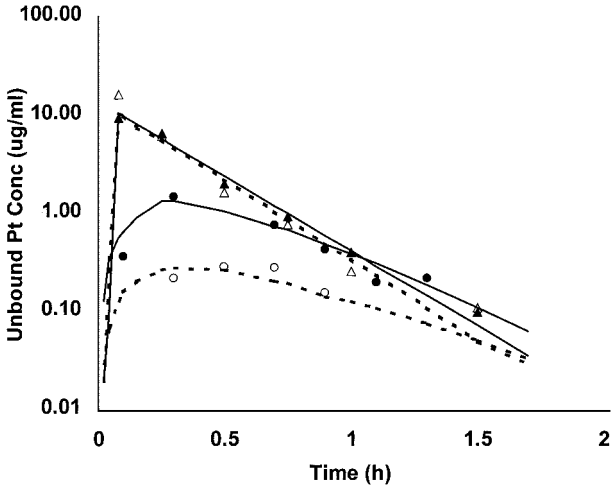

Fig. 2 Representative concentration *versus* time plots of unbound Pt in plasma and tumor ECF tumors after giving cisplatin at 10 mg/kg to mice bearing B16 and H23 tumors. The concentration of Pt measured in each 12-min sample of tumor ECF represents the average concentration of that interval. Therefore, data are plotted at the midpoint of that interval (*i.e.*, 0.1, 0.3, 0.5, 0.7, 0.9, 1.1, 1.3, 1.5, 1.7, and 1.9 h). Individual data and best fit line for unbound Pt concentration *versus* time profiles in plasma (▲) and tumor ECF (●) of mice bearing B16 murine melanoma tumors are presented. Individual data and best fit line for unbound Pt concentration *versus* time profiles in plasma (△) and tumor ECF (○) of mice bearing H23 human NSCLC xenografts are also presented.

0.7, 0.9, 1.1, 1.3, 1.5, 1.7, and 1.9 h). During collection of ECF after administration of cisplatin, Ringer's solution, USP without cisplatin, was perfused through the probe at 2 μl/min. The microdialysis samples were stored at 4°C until analyzed for Pt by FAAS (12, 13).

At the end of the microdialysis procedure, tumor samples were obtained at each probe site and analyzed for total Pt. Tumor homogenates were processed, and total Pt was analyzed by FAAS as described above. In addition, bifunctional intrastrand DNA adducts between Pt-GG and between Pt-AG were measured in B16 tumor samples from mice treated with 3 or 10 mg/kg of cisplatin. A ^{32}P-postlabeling assay was used to quantitate Pt-GG and Pt-AG Pt-DNA adducts (14).

Pharmacokinetic Analysis. ADAPT II was used to fit a two-compartment pharmacokinetic model, with uncoupled distribution of the plasma and tumor compartments, to the plasma and tumor ECF concentration-time profiles of unbound Pt (Ref. 15; Fig. 1). The estimated systemic parameters for unbound Pt included volume of the central compartment (V_c) and elimination rate constant (k_{10}; Ref. 15). The estimated model for the plasma concentration *versus* time data was then used to represent the time course of drug delivery to the tumor. Using a standard modeling framework and modeling the plasma and tumor disposition simultaneously, accurate estimates of the rate constant describing the movement of drug into the tumor ECF or the volume of the ECF were not possible (15). Thus, uptake and disposition in the tumor ECF were modeled separately as shown in Fig. 1 (15, 16). The equation defining the concentration of unbound-Pt in tumor ECF was derived as follows:

$$dA_{ECF}/dt = k_{P-ECF} \times A_p - k_{ECF-P} \times A_{ECF} \quad (1)$$

$$(dA_{ECF}/dt) \times 1/V_{ECF} = [(k_{P-ECF} \times A_p) - (k_{ECF-P} \times A_{ECF})]\, x^1/V_{ECF} \quad (2)$$

$$dC_{ECF}/dt = (k_{P-ECF}/V_{ECF}) \times A_p - k_{ECF-P} \times C_{ECF} \quad (3)$$

In equation 3, C_{ECF} (ng/ml) denotes the concentration of unbound Pt in the tumor ECF, $k_{P\text{-}ECF}$ (h^{-1}) is the rate of transfer of unbound Pt from plasma into tumor ECF, V_{ECF} (ml) is the volume of tumor ECF, $k_{ECF\text{-}P}$ (h^{-1}) is the rate constant of transport of unbound Pt out of tumor ECF, and A (ng) represents the fitted exponential function describing the amount of unbound Pt in the plasma. The $k_{ECF\text{-}P}$ (h^{-1}) represents the summation of the movement of drug from the tumor ECF. The model represented by equation 3 was fit to the concentrations of unbound Pt in the tumor ECF. For each animal and each tumor type, the maximum likelihood estimates of the ratio $k_{P\text{-}ECF}/V_{ECF}$ [plasma to tumor ECF transport rate constant:unit volume (ml) of tumor] and $k_{ECF\text{-}P}$ were obtained.

The pharmacokinetic model was used to calculate the systemic clearance of unbound Pt (CL) and area under the plasma (AUC_P) and tumor ECF (AUC_{ECF}) concentration-time curves of unbound Pt from time zero to infinity (15, 17). The penetration of unbound Pt into the tumor ECF was calculated as the ratio of AUC_P to AUC_{ECF} (3, 16).

Factor VIII Determination. To determine one potential factor that could affect Pt exposure in tumors, the degree of tumor vascularity, as measured by Factor VIII expression, was assessed after administration of cisplatin at 10 mg/kg to mice bearing B16 tumors and H23 xenografts (18, 19). After the end of the microdialysis procedure, a tumor section was obtained at each probe site and evaluated for Factor VIII expression by immunohistochemistry. Rabbit antihuman von Willebrand Factor (Factor VIII) antibody (Code A0082; DAKO Corp., Carpinteria, CA) was used to detect Factor VIII according to the manufacturer's recommendations. Biotinylated goat antirabbit

Table 1 Pharmacokinetic parameters for unbound Pt after cisplatin administration

		B16 murine melanoma				H23 NSCLC	
		3 mg/kg		10 mg/kg		10 mg/kg	
Parameter	Units	Mean ± SD	Median (range)	Mean ± SD	Median (range)	Mean ± SD	Median (range)
AUC_P	μg/ml·h	1.0		3.9		3.8	
CL	liter/h/m^2	616		500		435	
k_{10}	h^{-1}	1.7		2.3		3.5	
V_c	liter/m^2	234		143		82	
$k_{P\text{-}ECF}/V_{ECF}$	h^{-1}/liter/m^2	0.011 ± 0.005	0.009 (0.004–0.018)	0.003 ± 0.002	0.002 (0.0001–0.006)	0.002 ± 0.002	0.001 (0.001–0.006)
$k_{ECF\text{-}P}$	h^{-1}	4.8 ± 1.6	5.1 (2.4–7.6)	2.4 ± 0.8	2.4 (1.3–4.3)	2.5 ± 1.9	2.3 (0.4–6.2)

antibody with avidin-biotin complex and 3,3′-diaminobenzidine were purchased as the Vectastain Elite Kit (Vector Labs) and used according to the manufacturer's recommendation (20).

Image analysis was performed using Oncor Image Software (Oncor, Gaithersburg, MD). An Axiovert 10 Zeiss microscope equipped with CCD and Sit video cameras were coupled to the image analysis system. Slides were examined under low power and data from four fields near the probe placement were acquired. Erythrocytes from a healthy human donor, and confirmed to be of normal volume, were used to calibrate the analysis system. The area (μm^2) of the Factor VIII-positive-staining blood vessels in each section was calculated from the total number of pixels using a conversion factor of 6.25. The tumor vascularity was calculated as the ratio of Factor VIII labeled area to the total area of field multiplied by 100 (*i.e.*, percentage of Factor VIII).

Statistical Analysis. The Wilcoxon's rank-sum test was used to compare tumor vascularity, AUC_{ECF}, and total Pt in homogenates in mice bearing B16 tumors and H23 xenografts treated with 10 mg/kg of cisplatin. StatXact-3 software (Cytel, Inc., Cambridge, MA) was used for all statistical analyses.

RESULTS

***In Vivo* Probe Recovery.** The *in vivo* recovery values for Pt as measured by the retrodialysis method were 29 ± 7% and 44 ± 7% in B16 and H23 tumors, respectively. In addition, the ratios of *in vivo* recovery from probe A to probe B in B16 and H23 tumors were 0.77 ± 0.16 and 1.00 ± 0.29, respectively. The variability of *in vivo* recovery may be associated with differences in tumor blood flow, capillary permeability, and other factors that may alter the concentration-dependent passive diffusion of substances across the semipermeable microdialysis membrane (3). Pt was not detectable in any dialysate sample collected at the end of the washout period. Studies were excluded from analysis if the probe was broken, dislodged from the tumor, or in an area of the tumor where gross blood pooling occurred ($n = 4$ of 20 in B16 at 10 mg/kg; $n = 6$ of 16 in B16 at 3 mg/kg; and $n = 4$ of 14 in H23).

Pt Systemic and Tumor Disposition. Representative concentration *versus* time plots of unbound Pt in plasma and tumor ECF in mice bearing B16 tumors and H23 tumors after administration of cisplatin at 10 mg/kg are presented in Fig. 2. The plasma concentration *versus* time profiles of unbound Pt were similar in mice bearing B16 and H23 tumors and exhibited an elimination phase that is consistent with a one-compartment model. In mice bearing B16 and H23 tumors, the concentrations of unbound Pt in tumor ECF peaked at ~0.5 h after administration. In both tumor lines, the tumor ECF concentration *versus* time profile of unbound Pt did not parallel the plasma concentration *versus* time profile of unbound Pt. The concentrations of unbound Pt in the tumor ECF of the B16 tumors were ~2-fold higher than in the H23 tumors.

Pharmacokinetic parameters for unbound Pt in mice bearing B16 tumors after administration of cisplatin at 3 and 10 mg/kg and in mice bearing H23 tumors after administration of cisplatin at 10 mg/kg are presented in Tables 1 and 2. The percentage of unbound Pt AUC_P and AUC_{ECF} extrapolated was <10% in all groups, and therefore, the AUCs reported are from time zero to infinity (17, 21). After giving cisplatin at 3 and 10 mg/kg to mice bearing B16 murine melanoma tumors, there was a proportional increase in unbound Pt AUC_P. However, there was not a proportional increase in the unbound Pt AUC_{ECF} after giving cisplatin at 3 and 10 mg/kg to mice bearing B16 tumors (Table 2). After giving cisplatin at 10 mg/kg to mice bearing B16 or H23 tumors, the unbound Pt AUC_P was similar (Table 1). However, the AUC_{ECF} in mice bearing B16 tumors was ~1.5-fold higher than that in the H23 tumors (Table 2).

The unbound Pt AUC_{ECF}, total Pt, and Pt-DNA adducts in tumors and ratio of each from probe A to B in B16 and H23 tumors are presented in Table 2. The relatively high inter- and low intratumoral variability in the unbound Pt AUC_{ECF} in B16 and H23 tumors after administration of cisplatin at 10 mg/kg are presented in Fig. 3. In B16 tumors the inter- and intratumoral variability was ~30- and 2.5-fold, respectively. The relatively high inter- and low intratumoral variability in the total Pt concentration in B16 and H23 tumors after administration of cisplatin at 10 mg/kg is presented in Fig. 4. The intertumoral variability in the exposure of total Pt was less than that of unbound Pt in tumor ECF, however, the intertumoral variability of total Pt was still ~2-fold greater than the intratumoral variability. There was no relationship between tumor weight and AUC_{ECF} and total Pt.

The concentrations of total Pt in plasma, tumors, kidney, liver, and spleen in mice bearing B16 and H23 tumors are presented in Table 3. The concentrations of total Pt in all tissues peaked within 15 min after administration and remained relatively constant. The highest concentrations of total Pt were in the kidney and liver. The ratio of total Pt concentration in tumor compared with kidney was 0.2 to 0.3.

Table 2 Inter- and intratumor disposition of Pt after cisplatin administration

Tumor line (dose)	Intratumor comparsion	AUC_{ECF} (μg/ml·h)	Total Pt tumor (μg/gm)	Pt-GG DNA adducts (fmol/μg DNA)	Pt-AG DNA adducts (fmol/μg DNA)
B16 (3 mg/kg)		0.45 ± 0.13[a] 0.43 (0.25–0.75)	0.78 ± 0.27 0.84 (0.31–1.15)	5.2 ± 1.1 5.5 (3.1–6.6)	0.7 ± 0.1 0.7 (0.5–0.8)
	Ratio Probe A:B	1.3 ± 0.2 1.4 (1.1–1.6)	2.1 ± 0.9 2.0 (1.1–3.1)	1.2 ± 0.2 1.2 (1.0–1.5)	1.1 ± 0.1 1.1 (1.0–1.2)
B16 (10 mg/kg)		0.61 ± 0.48 0.42 (0.05–1.57)	1.6 ± 0.8 1.7 (0.2–2.5)	13.1 ± 3.3 13.2 (8.4–20.1)	2.2 ± 0.6 2.3 (1.3–3.2)
	Ratio Probe A:B	2.4 ± 1.3 1.8 (1.3–5.6)	1.3 ± 0.3 1.1 (1.0–2.0)	1.4 ± 0.4 1.3 (1.0–2.2)	1.4 ± 0.3 1.3 (1.1–2.1)
H23 (10 mg/kg)		0.33 ± 0.13 0.28 (0.18–0.53)	1.4 ± 0.3 1.3 (1.1–2.0)		
	Ratio Probe A:B	1.7 ± 0.7 1.5 (1.1–2.7)	1.3 ± 0.2 1.2 (1.1–1.6)		

[a] Mean ± SD, median, and range.

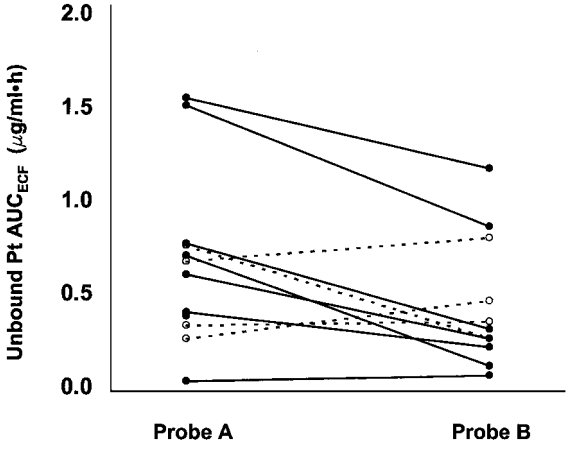

Fig. 3 Inter- and intratumoral variability in unbound Pt AUC_{ECF} in mice bearing B16 tumors and in mice bearing H23 xenografts after administration of cisplatin at 10 mg/kg. In mice bearing B16 murine melanoma tumors, individual AUCs are represented by ●, and AUCs within the same tumor are connected by ———. In mice bearing H23 human NSCLC xenografts, individual AUCs are represented by ○, and AUCs within the same tumor are connected by — — —.

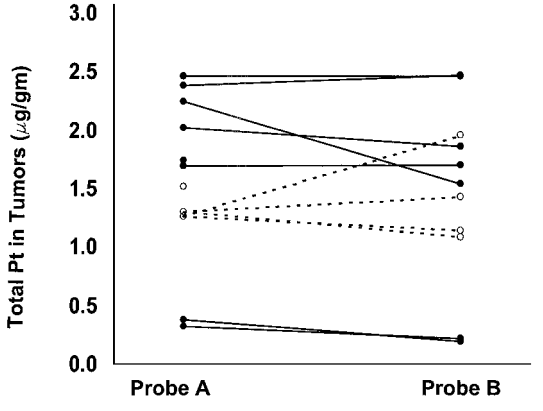

Fig. 4 Inter- and intratumoral variability in total Pt in mice bearing B16 tumors and in mice bearing H23 xenografts after administration of cisplatin at 10 mg/kg. In mice bearing B16 murine melanoma tumors, individual total Pt concentrations in tumor homogenates are represented by ●, and total Pt concentrations in tumor homogenates within the same tumor are connected by ———. In mice bearing H23 human NSCLC xenografts, individual total Pt concentrations in tumor homogenates are represented by ○, and total Pt concentrations in tumor homogenates within the same tumor are connected by — — —.

Pt-DNA Adduct Formation. To determine the factors associated with the formation of Pt-DNA adducts, the relationships between unbound Pt in tumor ECF (AUC_{ECF}), total Pt in tumor homogenates, and formation of Pt-GG and Pt-AG DNA adducts in mice bearing B16 tumors were evaluated. There was a poor relationship (R^2 = 0.21 and 0.22, respectively) between total Pt in tumor homogenates and the formation of Pt-GG and Pt-AG DNA when using a linear or Emax model to describe the relationship. However, when an Emax model was used to describe the relationship between tumor exposure to unbound Pt in tumor ECF and the formation of Pt-DNA adducts, there was a better correlation between unbound Pt AUC_{ECF} and Pt-GG (R^2 = 0.33) and Pt-AG (R^2 = 0.36) DNA adducts. The relationship between unbound Pt AUC_{ECF} and Pt-GG is presented in Fig. 5. In addition, there was a poor relationship between total Pt in tumor homogenates and unbound Pt AUC_{ECF} (R^2 = 0.05). There was no relationship between tumor weight and formation of Pt-DNA adducts.

Tumor Vascularity and Tumor Pt Exposure. The mean ± SD (median, range) tumor vascularity in B16 (n = 15) and H23 (n = 8) tumors was 1.8 ± 1.0 (1.9, 0.4–3.3%) and 1.0 ± 1.1% (0.3, 0.01–3.3%), respectively ($P < 0.05$). The mean ± SD (median, range) fold-difference in tumor vascularity within B16 and

Table 3 Total Pt concentrations after cisplatin administration

Tumor (dose)	Time point (min)	Plasma (μg/g)	Tumor (μg/g)	Liver (μg/g)	Kidney (μg/g)	Spleen (μg/g)
B16 (3 mg/kg)	5	2.32 ± 0.96[a]	2.18 ± 0.18	3.32 ± 0.39	3.87 ± 1.17	0.67 ± 0.03
	10	1.72 ± 0.87	1.83 ± 0.03	3.58 ± 0.33	4.97 ± 1.46	0.72 ± 0.12
	15	1.35 ± 0.27	1.66 ± 0.32	3.30 ± 0.16	1.90 ± 0.41	0.48 ± 0.17
	30	0.70 ± 0.07	1.60 ± 0.31	2.91 ± 0.46	2.36 ± 1.32	0.54 ± 0.13
	45	0.37 ± 0.06	0.81 ± 0.18	2.82 ± 0.39	3.07 ± 0.24	0.36 ± 0.04
	60	0.29 ± 0.01	0.91 ± 0.10	2.60 ± 0.38	2.95 ± 0.39	0.42 ± 0.07
	90	0.27 ± 0.03	1.40 ± 0.40	2.62 ± 0.06	2.86 ± 0.07	0.49 ± 0.11
	120	0.28 ± 0.04	1.54 ± 0.50	2.29 ± 0.21	2.48 ± 0.36	0.42 ± 0.03
B16 (10 mg/kg)	5	14.24 ± 5.69	3.23 ± 1.93	8.74 ± 2.73	23.69 ± 6.83	2.60 ± 0.23
	15	8.02 ± 1.97	2.23 ± 0.54	9.38 ± 2.85	19.13 ± 2.50	1.84 ± 0.34
	30	3.43 ± 0.57	3.08 ± 0.46	5.89 ± 1.10	15.87 ± 2.16	2.53 ± 0.37
	45	2.20 ± 0.46	2.61 ± 0.35	7.92 ± 3.51	13.38 ± 3.01	2.06 ± 0.61
	60	1.64 ± 0.12	1.89 ± 0.12	9.01 ± 3.32	11.79 ± 0.95	1.54 ± 0.33
	90	1.54 ± 0.18	2.68 ± 0.37	11.38 ± 1.4	11.32 ± 1.12	1.81 ± 0.30
	120	1.69 ± 0.05	2.05 ± 0.24	9.40 ± 0.44	15.79 ± 2.01	1.73 ± 0.53
H23 (10 mg/kg)	5	12.73 ± 3.02	3.56 ± 0.99	6.53 ± 1.84	11.30 ± 6.43	2.42 ± 0.77
	10	6.25 ± 0.28	3.34 ± 0.23	7.59 ± 2.70	8.46 ± 4.03	2.07 ± 0.05
	15	5.04 ± 0.70	4.26 ± 0.87	8.41 ± 2.02	12.27 ± 3.07	1.91 ± 0.28
	30	1.87 ± 0.31	2.79 ± 0.48	8.18 ± 0.39	7.17 ± 2.69	1.61 ± 0.31
	45	1.66 ± 0.44	3.00 ± 1.00	6.54 ± 1.56	7.47 ± 1.41	1.70 ± 0.43
	60	1.28 ± 0.05	3.44 ± 0.96	5.93 ± 1.57	6.65 ± 2.14	1.46 ± 0.24
	90	1.16 ± 0.12	3.96 ± 1.12	6.56 ± 2.33	6.93 ± 0.13	1.44 ± 0.12
	120	0.48 ± 0.13	4.07 ± 0.65	5.94 ± 2.77	7.19 ± 0.81	1.18 ± 0.43

[a] Mean ± SD.

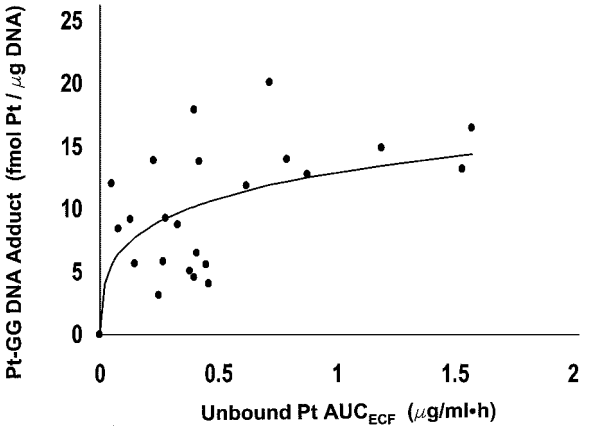

Fig. 5 Relationship between unbound Pt AUC_{ECF} and Pt-GG DNA adducts in mice bearing B16 tumors after administration of cisplatin at 3 and 10 mg/kg. Individual data points are presented as ●, and best fit line using an Emax model for the data are represented by ———.

H23 tumors was 3.3 ± 2.2 (2.2, 1.2–8.4) and 2.8 ± 1.1 (2.6, 1.6–4.9), respectively ($P > 0.05$). Tumor vascularity did not correlate with total Pt in tumor extracts ($R^2 < 0.03$) or unbound Pt AUC_{ECF} ($R^2 < 0.02$) for either B16 or H23 tumors.

DISCUSSION

Although many studies have evaluated the cellular uptake and accumulation of Pt and the formation of Pt-DNA adducts in *in vitro* studies, this is the first *in vivo* study that evaluates the relationship between unbound Pt exposure in tumor ECF as measured by microdialysis, total Pt in tumor homogenates, and the formation of Pt-DNA adducts (14). This is also the first study evaluating the inter- and intratumoral variability in Pt exposure after administration of cisplatin and the relationship between Pt exposure in tumor and tumor vascularity. After giving cisplatin at 3 and 10 mg/kg to mice bearing B16 tumors, there was a proportional increase in the unbound Pt AUC_P, however, there was not a proportional increase in AUC_{ECF} (Tables 1 and 2). There was relatively high (30-fold) inter- and low (2.5-fold) intratumoral variability in unbound Pt in tumor ECF and total Pt in tumor homogenates. Formation of Pt-GG and Pt-AG DNA adducts was better correlated with unbound Pt in tumor ECF than with total Pt. Tumor vascularity, as measured by Factor VIII expression, was a poor predictor of Pt tumor exposure within B16 or H23 tumors. However, Factor VIII expression may be a predictor of drug exposure between tumors.

The relatively high inter- and low intratumoral variability in Pt exposure in tumors may help to explain why in a patient with solid tumors such as melanoma and NSCLC there may be a reduction in the size of some lesions, whereas others progress during or after treatment, although the biology or genetic makeup of the tumors are similar (4). The greater inter- and intratumoral variability in unbound Pt in tumor ECF as compared with total Pt may be a result of differences in binding of Pt to proteins in the ECF and the tumor matrix (12, 13, 22).

Plasma concentrations are often used as a marker of cytotoxic exposure, however, drug delivery to the tumor is determined not only by plasma concentrations but also by the distribution from the plasma into the ECF of the tumor and from the ECF into the cells (2, 3, 23, 24). Solid tumors have several potential barriers to drug delivery that may limit drug penetration and provide inherent mechanisms of resistance. Moreover, factors affecting drug exposure in tissue such as alterations in the distribution of blood vessels, blood flow, capillary permeability, interstitial pressure, and lymphatic drainage may vary in

tumors (2, 3). The surrounding tissue environment also influences the microcirculation of tumors, and thus, melanoma tumors located in the skin or lung, or NSCLC located in the lung or brain, may have significantly different exposures to drug (25, 26). In addition, highly malignant uveal melanomas have blood vessels produced by the melanoma cells themselves in addition to blood vessels recruited from the surrounding tissue (26–29). Thus, there are several highly complicated factors affecting the delivery of anticancer agents to the primary tumor and metastases in patients with solid tumors (2, 25, 26, 29).

In our study, tumor vascularity, as measured by Factor VIII expression, was a poor predictor of Pt tumor exposure within B16 or H23 tumors. In addition, the difference in tumor vascularity (1.8 ± 1.0 and 1.0 ± 1.1%, respectively, $P < 0.05$) between B16 and H23 did not translate into difference in unbound Pt AUC_{ECF} (0.6 ± 0.5 and 0.3 ± 0.1 μg/ml·hr, respectively, $P > 0.05$) or total Pt in tumor homogenates (1.6 ± 0.8 and 1.3 ± 0.3 g/g, respectively, $P > 0.05$) between the tumor lines. A possible limitation of Factor VIII expression, an anatomical marker of vascularity, is that it does not measure differences in drug delivery based on capillary permeability or interstitial pressure (2, 18, 19, 30, 31). Physiological measures of drug delivery into tumors and lymphatic drainage from tumors such as ^{99m}Tc-diethylenetriaminepentaacetic acid and ^{99m}Tc-sulfur colloid, respectively, may be better correlates of drug exposure in tumors (30–34).

Using an Emax model to describe the relationship between drug exposure and Pt-DNA adduct formation, there was a better correlation between the formation of Pt-GG and Pt-AG DNA adducts and unbound Pt in tumor ECF than with total Pt measured in tumor homogenates. These data suggest that after administration of cisplatin, the unbound Pt in tumor ECF is a better measure of the active drug exposure in tumors than is total Pt measured in tumor extracts. Consistent with this theory, our previous studies of pegylated-liposomal cisplatin formulations suggest these agents distribute into tumors but release significantly less Pt into tumor ECF, which results in the formation of fewer Pt-DNA adducts compared with cisplatin (35). In addition, we have previously reported a 3.5-fold difference in the tumor ECF exposure of topotecan between resistant and sensitive human neuroblastoma (3). This difference in topotecan exposure in tumor ECF was consistent with other studies reporting a 6-fold difference in topotecan dose and systemic exposure, achieving a complete response in these two neuroblastoma tumor lines (3, 36). Our results suggested that topotecan tumor penetration and ECF exposure might be one factor associated with antitumor response. The need for an Emax model to describe the relationship suggests there is saturation in the formation of Pt-DNA adducts with increasing unbound Pt exposure in the tumor. Previous studies have also reported saturation in the formation of Pt-DNA adducts with increasing exposures of cisplatin and carboplatin (37, 38).

Although we have previously reported the relationship between topotecan ECF exposure and antitumor response in mice bearing human neuroblastoma xenografts (3), this is the first study modeling the tumor ECF concentration *versus* time profile separately from the systemic disposition to describe the tumor ECF disposition of an anticancer agent. The systemic disposition of unbound Pt in plasma after administration of cisplatin is most adequately described by a one-compartment pharmacokinetic model (15). Adding a second standard tissue compartment with intercompartmental rate constants to describe the distribution of unbound Pt into the tumor ECF does not accurately reflect the single phase elimination of unbound Pt in plasma (12, 13, 22). The term ($k_{P\text{-}ECF}/V_{ECF}$) describing the movement of unbound Pt from the blood into tumor was 100- to 1000-fold less than the rate constant (k_{10}) describing the systemic elimination of unbound Pt. Because of this 100- to 1000-fold difference between the rate constants describing systemic and tumor disposition of unbound Pt, the pharmacokinetic model could not accurately estimate these parameters simultaneously (15). In addition, the movement of drug into the tumor is significantly less than the elimination of drug from the body. Therefore, the tumor disposition of drug does not significantly affect the systemic drug disposition, and as a result, it can be modeled separately from the systemic disposition. Application of this pharmacokinetic model with uncoupled distribution of drug to tumor ECF provides a mathematical model to describe the differences in the disposition of chemotherapeutic agents in tumor ECF. Moreover, pharmacokinetic models with uncoupled distribution of drug in peripheral compartments can be used to describe drug disposition in tissue and the central nervous system (16).

The clinical relevance of these studies reflects the need to determine the reasons for variable tumor response within a patient and the importance of drug delivery into the tumor (2, 3, 23, 24). In addition, effort is needed to uncover reasons why chemotherapeutic agents that show encouraging promise in preclinical *in vitro* and *in vivo* studies often produce minimal or no effect in the clinical treatment of common solid tumors (1). Xenograft tumor models may not accurately reflect solid tumors in patients because of differences in growth characteristics, vasculature, and the lack of lymphatic drainage in flank tumor models (27, 36, 39). Thus, to effectively determine the influence of drug delivery to tumors on antitumor response, studies evaluating the inter- and intratumoral variability have to be performed in patients with solid tumors (5–7). In addition, evaluating the disposition of anticancer agents in tumors of patients compared with xenograft models may also determine whether xenograft models implanted in the flank of mice are relevant models of antitumor effect (36, 39, 40).

REFERENCES

1. Grever, M. R., and Chabner, B. A. Cancer drug development. *In:* V. T. DeVita, S. Hellman, and S. A. Rosenberg (eds.), Cancer: Principles and Practice of Oncology, Ed. 5, p. 385. Philadelphia: Lippincott-Raven, 1997.

2. Jain, R. K. Delivery of molecular medicine to solid tumors. Science (Wash. DC), *271:* 1079–1080, 1996.

3. Zamboni, W. C., Houghton, P. J., Hulstein, J. L., Kirstein, M., Walsh, J., Cheshire, P. J., Hanna, S. K., Danks, M. K., and Stewart, C. F. Relationship between tumor extracellular fluid exposure to topotecan and response in human neuroblastoma xenografts and cell lines. Cancer Chemother. Pharmacol., *43:* 269–276, 1999.

4. Balch, C. M., Reintgen, D. S., Kirkwood, J. M. Cutaneous melanoma. *In:* V. T. DeVita, S. Hellman, and S. A. Rosenberg (eds.), Cancer: Principles and Practice of Oncology, Ed. 5, p. 1947, Philadelphia: Lippincott-Raven, 1997.

5. Muller, M., Mader, R. M., Steiner, B., Steger, G. G., Jansen, B., Gnant, M., Helbich, T., Jakesz, R., Eichler, H. G., and Blochl-Daum, B. 5-Fluorouracil kinetics in the interstitial tumor space: clinical response in breast cancer patients. Cancer Res., *57:* 2598–2601, 1997.

6. Blochl-Daum, B., Muller, M., Meisinger, V., Eichler, H. G., Fassolt, A., and Pehamberger, H. Measurement of extracellular fluid carboplatin kinetics in melanoma metastases with microdialysis. Br. J. Cancer, *73:* 920–924, 1996.

7. Muller, M., Schmid, R., Georgopoulos, A., Buxbaum, A., Wasicek, C., and Eichler, H. G. Application of microdialysis to clinical pharmacokinetics in humans. Clin. Pharmacol. Ther., *57:* 371–380, 1995.

8. Johansen, M. J., Newman, R. A., and Madden, T. The use of microdialysis in pharmacokinetics and pharmacodynamics. Pharmacotherapy, *17:* 464–481, 1997.

9. Kehr, J. A survey on quantitation microdialysis: theoretical models and practical limitations. J. Neurosci. Methods, *48:* 251–261, 1993.

10. National Research Council. Guide to the Care and Use of Laboratory Animals. Washington, DC: National Academy Press, 1996.

11. Conley, B. A., Ramsland, T. S., Sentz, D. L., Wu, S., Rosen, D. M., Wollman, M., and Eiseman, J. L. Antitumor activity, distribution, and metabolism of 13-*cis*-retinoic acid as a single agent or in combination with tamoxifen in established human MCF-7 xenografts in mice. Cancer Chemother. Pharmacol., *43:* 183–197, 1999.

12. Erkmen, K., Egorin, M. J., Reyno, L. M., Morgan, R., Jr., and Doroshow, J. H. Effects of storage on the binding of carboplatin to plasma protein. Cancer Chemother. Pharmacol., *35:* 254–256, 1995.

13. Egorin, M. J., Van Echo, D. A., Tipping, S. J., Olman, E. A., Whitacre, M. Y., Thompson, B. W., and Aisner, J. Pharmacokinetics and dosage reduction of *cis*-diammine(1,1-cyclobutanedicarboxylato) platinum in patients with impaired renal function. Cancer Res., *44:* 5432–5438, 1984.

14. Pluim, D., Maliepaard, M., van Waardenburg, R. C., Beijnen, J. H., and Schellens, J. H. M. 32P-postlabeling assay for the quantitation of the major platinum-DNA adducts. Anal. Biochem., *274:* 30–38, 1999.

15. D'Argenio, D. Z., and Schumitzky, A. A program package for simulation and parameter estimation in pharmacokinetic systems. Comput. Programs Biomed., *9:* 115, 1979.

16. Zamboni, W. C., Luftner, D. I., Egorin, M. J., Schweigert, M., Sezer, O., Richter, T., Natale, J. J., and Possinger, K. The effect of increasing topotecan infusion from 30 minutes to 4 hours on the duration of exposure in cerebrospinal fluid. Ann. Oncol., *12:* 119–122, 2001.

17. Gibaldi, M., and Perrier, D. (eds). Pharmacokinetics, 2nd Edition, pp. 445–457. NY: Marcel Dekker, 1982.

18. Mukai, K., Rosai, J., and Brugdorf, W. H. C. Localization of factor VIII-related antigen in vascular endothelial cells using an immunoperoxidase method. Am. J. Surg. Pathol., *4:* 273–276, 1980.

19. McComb, R. D., Jones, T. R., Pizzo, S. V., and Bigner, D. D. Specificity and sensitivity of immunohistochemical detection of factor VIII/von Willebrand Factor antigen in formalin-fixed paraffin-embedded tissue. J. Histochem. Cytochem., *30:* 371–377, 1982.

20. Malafa, M. P., Barnett, J. M., Karich, T., Neitzel, L., and Webb, B. Angiogenesis does not correlate with rectal cancer metastasis. J. Appl. Res., *1:* 1–7, 2001.

21. Zamboni, W. C., Bowman, L. C., Tan, M., Santana, V. M., Houghton, P. J., Meyer, W. H., Pratt, C. B., Heideman, R. L., Gajjar, A. J., Pappo, A. S., and Stewart, C. F. Interpatient variability in bioavailability of the intravenous formulation of topotecan given orally to children with recurrent solid tumors. Cancer Chemother. Pharmacol., *43:* 454–460, 1999.

22. Gerad, H., Egorin, M. J., Whitacre, M., Van Echo, D. A., and Aisner, J. Renal failure and platinum pharmacokinetics in three patients treated with *cis*-diamminedichloroplatinum(II) and whole-body hyperthermia. Cancer Chemother. Pharmacol., *11:* 162–166, 1983.

23. Boucher, Y., and Jain, R. K. Microvascular pressure is the principal driving force for interstitial hypertension in solid tumors: implication for vascular collapse. Cancer Res., *52:* 5110–5114, 1992.

24. Helmlinger, G., Yuan, F., and Jain, R. K. Interstitial pH and pO_2 gradients in solid tumors *in vivo*: high-resolution measurements reveal a lack of correlation. Nat. Med., *3:* 177–182, 1997.

25. Hobbs, S. K., Monsky, W. L., Yuan, F., Roberts, W. G., Griffith, L., Torchilin, V. P., and Jain, R. K. Regulation of transport pathways in tumor vessels: role of tumor type and microenvironment. Proc. Natl. Acad. Sci. USA, *95:* 4607–4612, 1998.

26. Barnhill, R. L. The biology of melanoma micrometastases. Recent Results Cancer Res., *158:* 3–13, 2001.

27. Graff, B. A., Bjornaes, I., and Rofstad, E. K. Microvascular permeability of human melanoma xenografts to macromolecules: relationships to tumor volumetric growth rat tumor angiogenesis, and VEGF expression. Microvasc. Res., *61:* 187–198, 2001.

28. Folberg, R., Chen, X., Boldt, H. C., Pe'er, J., Brown, C. K., Woolson, R. F., and Mani, A. J. Microcirculation patterns other than loops and networks in choroidal and ciliary body melanomas. Ophthalmology, *108:* 996–1001, 2001.

29. Maniotis, A. J., Folberg, R., Hess, A., Seftor, E. A., Gardner, L. M., Pe'er, J., Trent, J. M., Meltzer, P. S., and Hendrix, M. J. C. Vascular channel formation by human melanoma cells *in vivo* and *in vitro*: vasculogenic mimicry. Am. J. Pathol., *155:* 739–752, 1999.

30. Takamitsu, O., Tjuvajev, J. G., Miyagawa, T., Sasajima, T., Joshi, A., Joshi, R., Finn, R., Claffey, K. P., and Blasberg, R. G. Tumor growth modulation by sense and antisense vascular endothelial growth factor gene expression: effects on angiogenesis, vascular permeability, blood volume, blood flow, fluorodeoxyglucose uptake, and proliferation of human melanoma intracerebral xenografts. Cancer Res., *58:* 4185–4192, 1998.

31. Bjornaes, I., Lyng, H., Dahle, G. A., Kaalhus, O., and Rofstad, E. K. Intratumor heterogeneity in perfusion in human melanoma xenografts measured by contrast-enhanced magnetic resonance imaging. Magn. Reson. Imaging, *18:* 997–1002, 2000.

32. Karakousis, C. P., and Grigoropoulos, P. Sentinel node biopsy before and after wide excision of the primary melanoma. Ann. Surg. Oncol., *6:* 785–789, 1999.

33. Morton, D. L., Thompson, J. F., Essner, R., Elashoff, R., Stern, S. L., Nieweg, O. E., Roses, D. F., Karakousis, C. P., Mozzillo, N., Reintgen, D., Wang, H., Glass, E. C., Cochran, A. J., and the Multicenter Selective Lymphadenectomay Trial Group. Validation of the accuracy of intraoperative lymphatic mapping and sentinel lymphadenectomy for early-stage melanoma. Ann. Surg., *230:* 453–465, 1999.

34. Morton, D. L. Lymphatic mapping and sentinel lymphadenectomy for melanoma past, present, and future. Ann. Surg. Oncol., *8* (Suppl. 9)*:* 22S–28S, 2001.

35. Zamboni, W. C., Gervais, A. C., Schellen, J. H. M., Delauter, B. J., Egorin, M. J., Zuhowski, E. G., Pluim, D., Hamburger, D. R., Working, P. K., Colbern, G., and Eiseman, J. L. Disposition of platinum (Pt) in B16 murine melanoma tumors after administration of cisplatin and pegylated liposomal-cisplatin formulations (SPI-077 & SPI-077 B103) (Abstract). Proceedings of 11th NCI-EORTC-AACR Symposium on New Drugs in Cancer Therapy, 2000.

36. Zamboni, W. C., Stewart, C. F., Thompson, J., Santana, V., Cheshire, P. J., Richmond, L. B., Lui, X., Houghton, J. A., and Houghton, P. J. The relationship between topotecan systemic exposure and tumor response in human neuroblastoma xenografts. J. Natl. Cancer Inst. (Bethesda), *90:* 505–511, 1998.

37. Chau, Q., and Stewart, D. J. Cisplatin efflux, binding, and intracellular pH in the HTB56 human lung adenocarcinoma cell line and the E-8/0.7 cisplatin-resistant variant. Cancer Chemother. Pharmacol., *44:* 193–202, 1999.

38. Veal, G. J., Dias, C., Price, L., Parry, A., Errington, J., Hale, J., Pearson, A. D. J., Boddy, A. V., Newell, D. R., and Tilby, M. J. Influence of cellular factors and pharmacokinetics on the formation of platinum-DNA adducts in leukocytes of children receiving cisplatin therapy. Clin. Cancer Res., *7:* 2205–2212, 2001.

39. Furman, W. L., Stewart, C. F., Poquette, C. A., Pratt, C. B., Santana, V. M., Zamboni, W. C., Bowman, L. C., Ma, M. K., Hoffer, F. A., Meyer, W. H., Pappo, A. S., Walter, M., and Houghton, P. J. Direct translation of protracted irinotecan schedule from a xenograft model to a Phase I trial in children. J. Clin. Oncol., *17:* 1815–1824, 1999.

40. Rodriguez-Galindo, C., Radomski, K., Stewart, C. F., Furman, W., Santana, V. M., and Houghton, P. J. Clinical use of topoisomerase I inhibitors in anticancer treatment. Med. Pediatr. Oncol., *35:* 385–402, 2000.